

pubs.acs.org/JACS Article

Reconfigurable DNA Nanocage for Protein Encapsulation and Regulation

Xu Chang, Qi Yang, Jung Yeon Lee, Devanathan Perumal, and Fei Zhang*



Cite This: J. Am. Chem. Soc. 2024, 146, 26131-26138



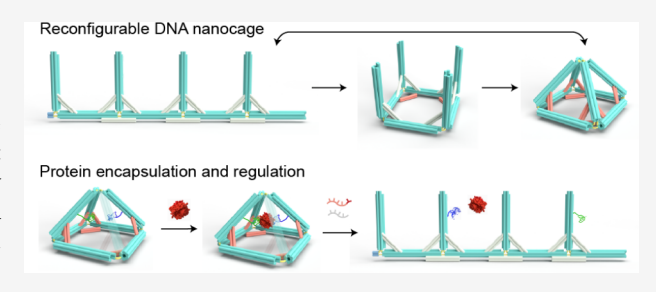
ACCESS I

Metrics & More

Article Recommendations

s Supporting Information

ABSTRACT: Creating nanomachines capable of precisely capturing, organizing, and regulating the activity of target biomolecules holds profound significance for advancing nanotechnology and therapeutics. Here, we develop a multistage reconfigurable DNA nanocage that can enclose and modulate proteins through multivalent interactions, activated by specific molecular signals. By strategically designing and manipulating the strut architecture of the DNA nanocages, we can achieve precise control over their reconfiguration among pyramid, square, and linear branch shapes. Additionally, we demonstrated its ability to capture thrombin and effectively inhibit its



coagulation activity by incorporating two thrombin-targeting aptamers into the designed arms of the DNA nanocage. The activity of thrombin can be recovered by rearranging the conformation of the DNA nanocage and exposing the protein, thereby activating the coagulation process. This approach enriches the design toolbox for dynamic nanomachines and inspires a new strategy for protein encapsulation and regulation with potential future therapeutic applications.

■ INTRODUCTION

In recent years, the fast development of DNA nanotechnology, particularly the DNA origami technique, has enabled the creation of precise nanostructures and spatial organization of molecules with nanometer accuracy.⁶⁻¹⁰ DNA origami is characterized by the use of a long scaffold DNA strand and hundreds of short staple strands that fold into predetermined 2D or 3D structures via a self-assembly process. It is convenient to introduce dynamic behavior into DNA origami using toehold-mediated strand displacement reactions. 11-17 Leveraging these capabilities, DNA origami has been instrumental in the development of dynamic nanodevices and nanorobots. 18-21 Examples range from tweezers, 22 rotators, 23,24 boxes, 12 to DNA walkers, 25 and cargo-sorting robots.¹⁹ Particularly, DNA origami nanorobots with proteins as guests have been demonstrated, such as a logic-gated DNA robot designed for targeted payload delivery, 13 a DNA nanovault for regulating enzyme-substrate interactions,² and a DNA nanotube for anticancer drug transport. A notable recent development is the DNA icosahedral shell system, which features 90 antibody binding sites, trapping virus particles and reducing viral infections.²⁸ Given that protein and enzyme activities are essential for biological functions, it is important to create synthetic nanodevices that can target and regulate protein activities for future medical applications. However, the creation of a reconfigurable DNA nanodevice that mimics protein regulation processes demands intricate dynamic designs and precise control over the parameters.

Inspired by the protein regulation process, we conceived the idea of building a reconfigurable DNA nanocage that controls the coagulation activity of thrombin by occupying and releasing its two exosite binding sites through conformational changes triggered by molecular inputs. The reconfiguration of DNA nanocages was achieved by employing the scaffold-strut design at the joint of the DNA helix bundles. The length of the strut was designated to support neighboring edges and to pull them to a certain angle during the reconfiguration. Struts have been established as practical units to stabilize the angles between DNA arms, such as building DNA polyhedral assembly,²⁹ or to control the distance between DNA helixes, such as in a DNA origami nanoactuator.³⁰ In this work, we successfully showcased the effective reconfiguration of DNA nanocages by altering their strut designs through strand displacement reactions. By adding open and close set strands to replace the staple DNA bound to the scaffold of the strut, we were able to adjust the distance between DNA bundle edges, thus switching the conformations of DNA nanocages between linear branch, square, and pyramid shapes.

We next used thrombin as a case study to illustrate the emulation of protein regulation through the reconfiguration of DNA nanocages. Thrombin plays a central role in blood clotting process, in which soluble fibringen is converted to

Received: May 20, 2024 Revised: September 2, 2024 Accepted: September 4, 2024 Published: September 14, 2024





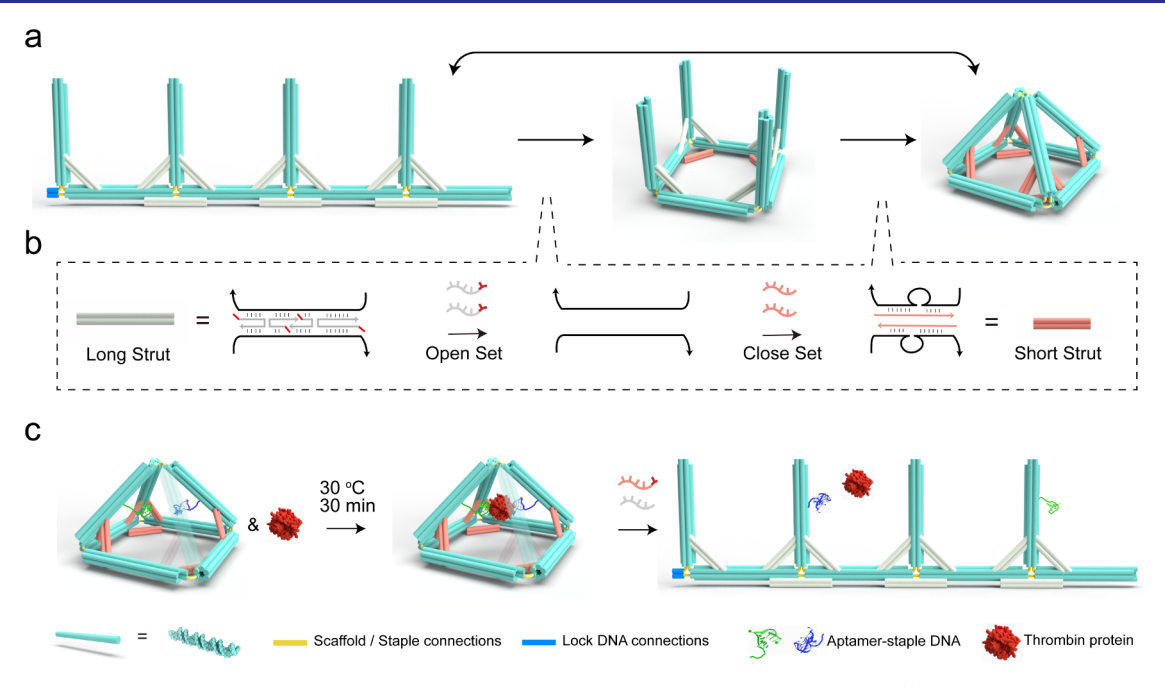


Figure 1. A strut enabled multistage reconfigurable DNA nanocage for protein caging and regulation. (a) Schematic representation of DNA nanocage transforming between linear branch shape, open square shape, and closed pyramid shape. The body of DNA nanocage is made of DNA six-helix bundle colored in cyan, while the strut is built by two double helical DNA. Three struts on the backbone are responsible for linear branch to open square transition, while seven bevel struts are involved in the open square to pyramid transition. Struts (long) before reconfiguration are labeled in silver color, while struts (short) after reconfiguration are colored pink. Cylinder model represents double helical DNA. (b) Schematics of controlling the length of strut. Scaffold DNA and staple DNA on the strut are represented by black line and silver line with arrow, respectively. Toehold region is highlighted in red on staples and in open set DNA. open set DNA will hybridize with staple DNA on long struts by toehold displacement reactions, followed by close set DNA binding parts of scaffold and extruding extra scaffold DNA to produce short struts. (c) 3D models of a pyramid DNA nanocage capturing and regulating human α-thrombin protein. Open set and close set DNA are added to rearrange the shape of DNA nanocage and recover the activity of thrombin. DNA aptamers are modified in two staple strands and protrude toward the cavity of DNA nanocage. One arm of DNA pyramid is rendered with transparency to show the aptamer-thrombin binding inside of the pyramid. Images of thrombin protein and DNA aptamers are prepared using SEW1.pdb. Sequences of staples strands, staple connection strands, lock DNA connection strands, and open and close sets DNA are listed in the Tables S3–S5 and S7.

insoluble fibrin network.31 In living systems, a deficiency of reactive thrombin will cause spontaneous bleeding, while the excess will lead to vein thrombosis. 32,33 Regulating the activity of individual thrombin molecules is essential to maintaining the overall active thrombin within a safe range. DNA aptamers, specifically TA-15 and TA-29, have been identified to bind exosite I and exosite II of thrombin, 34-36 respectively. By the incorporation of these aptamer sequences into the staples, the pyramid DNA nanocage was able to effectively encapsulate thrombin within its cavity through bivalent binding. Furthermore, an AND logic gate behavior was observed between aptamers functionalized DNA nanocage and the activity of thrombin, highlighting that neither the presence of a single aptamer nor the DNA nanocage alone could inhibit thrombin, due to the lack of bivalent encapsulation. 31,37 Notably, our reconfigurable DNA nanocage was able to respond to molecular modulators and recover the activity of thrombin in a manner that is akin to natural protein regulation. The enzyme reaction rate significantly increased upon the introduction of neutralizer or modulator DNA strands during real-time monitoring, showing the dynamic and responsive nature of our system.

RESULTS AND DISCUSSION

Design and Reconfiguration of the DNA Nanocage. The synthetic DNA nanocage is folded using the DNA origami technique² with three constructional parts: the main body of

the framework, DNA struts, and DNA connections. Taking the linear branch conformation (Figure 1a) as an example, the backbone and branched edges (cyan) are formed from DNA six-helix bundles to maintain structural integrity and provide space for strut designs. The scaffold DNA connections (yellow) route through each DNA six-helix bundle and connect two adjacent bundles at each joint. The second functional part is the DNA strut (silver and pink). Scaffold DNA route through two double-helical DNA and pull two sixhelix bundles together at a certain angle. Three such struts immobilize the angle of a joint in 3D, and a total of 10 struts fix the DNA nanorobot in one of the three configurations. The third component is the lock DNA connectors and staple DNA connectors in sapphire color and yellow, respectively. Lock DNA connectors are located at the joint with only one strut, and, as the name indicates, lock the head and tail of the backbone after reconfiguration to maintain the square and pyramid shape. Staple connectors serve the same role but are located at the vertex of the pyramid shape during the squareto-pyramid transition. The assembly of linear branch DNA nanocages at different Mg²⁺ concentrations was optimized and validated by agarose gel electrophoresis (Figure S2).

The conformational regulation of the DNA nanocage was achieved by dynamically changing the lengths of specific DNA struts corresponding to certain configurations. During the transition from a linear branch to a square configuration, three struts along the linear backbone (backbone struts) play a

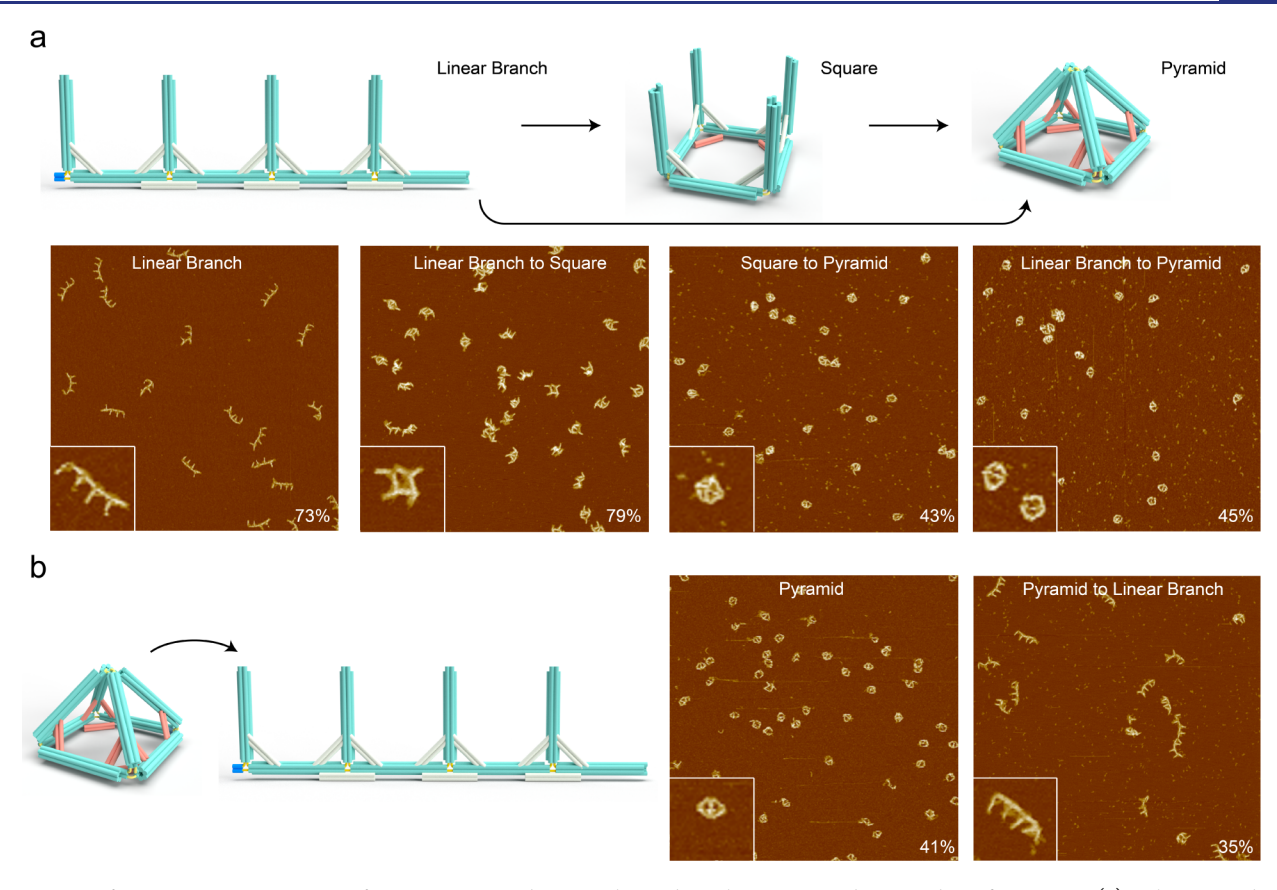


Figure 2. Conformation rearrangement of DNA nanocage between linear branch, square, and pyramid configurations. (a) Schemes and AFM images of stepwise and one-step reconfigurations. (b) Schemes and AFM images of pyramid DNA nanocage transforming to linear brach shape. Corresponding open set and close set were added in each step in (a) and (b). Size of AFM images: $2 \mu m \times 2 \mu m$, size of inset images 200 nm \times 200 nm. The numbers inside images are the yield of interested structures counting from AFM. Detailed information can be found in Supporting Figures S6–S11.

crucial role, whereas the remaining seven struts near the branches (bevel struts) facilitate the transformation from a square to a pyramid shape. Figure 1b shows the general principles for changing the lengths of DNA struts from long to short using strand displacements. The open set DNA strands loosen the strut by binding and removing the primer staple DNA on struts, while the close set DNA then hybridize with scaffold DNA, redefining the length of DNA struts by creating bulges with the unpaired scaffold DNA loops. The strut length for each specific configuration is calculated from the theoretical geometry of the configuration, where 10.5 nucleotide bases correspond to a length of 3.4 nm.

We demonstrated several reconfiguration processes of the DNA nanocage including step-by-step transformations from a linear branch to an open square and then to a pyramid shape and a one-step two-way transformation between the linear branch and the pyramid shape (Figure 1). DNA open set was added to relax struts, followed by the DNA close set, lock DNA connections or/and staple DNA connections to redefine those struts. Lock DNA connections and the DNA open set and close set of the backbone struts are involved in the linear branch-to-square transition, while the addition of staple connection strands and the DNA open set and close set of the bevel struts results in the reconfiguration from the square to the pyramid shape (Figure 1a,b). As for the two-way reconfigurations, open set DNA strands are added together to relax both the backbone and bevel struts of the linear branch shape at one time, followed by the close set, lock DNA

connections and staple connections, redefining these struts and transforming the nanocage to a pyramid shape. In the transition from pyramid nanocage to linear branch, a 6-base toehold is added to the struts of the pyramid to enable the opening and redefining processes. The Open and Close Set DNA in this transition changed accordingly.

Targeting moieties can be functionalized within the cavity of the pyramid DNA nanocage and enable the capture of biomolecules. We used the pyramid nanocage with aptamer modification to target thrombin protein and captured it from the solution by incubation. After the addition of the DNA open set and close set, DNA nanocages undergo a pyramid to linear branch shape transition and release the thrombin, thus restoring its activity (Figure 1c).

We validated the reconfiguration of a linear branch DNA nanocage using agarose gel and atomic force microscope (AFM). The linear branch DNA nanocage was initially folded by annealing and characterized by AFM. Next, we applied strand displacement reactions to change its conformation to a square and then to a pyramid with an option for a one-step transition directly to the pyramid. The products from each step were characterized using agarose gel electrophoresis and AFM (Figures 2a, S2, and S3). AFM images showed a clear conformation change from the linear branch to the square shape, where the straight backbone was reformed to a closed square with the branched arms deposited randomly on mica due to the flattening effect of the 3D structure under AFM tips. The pyramid-shaped DNA nanocages without opened

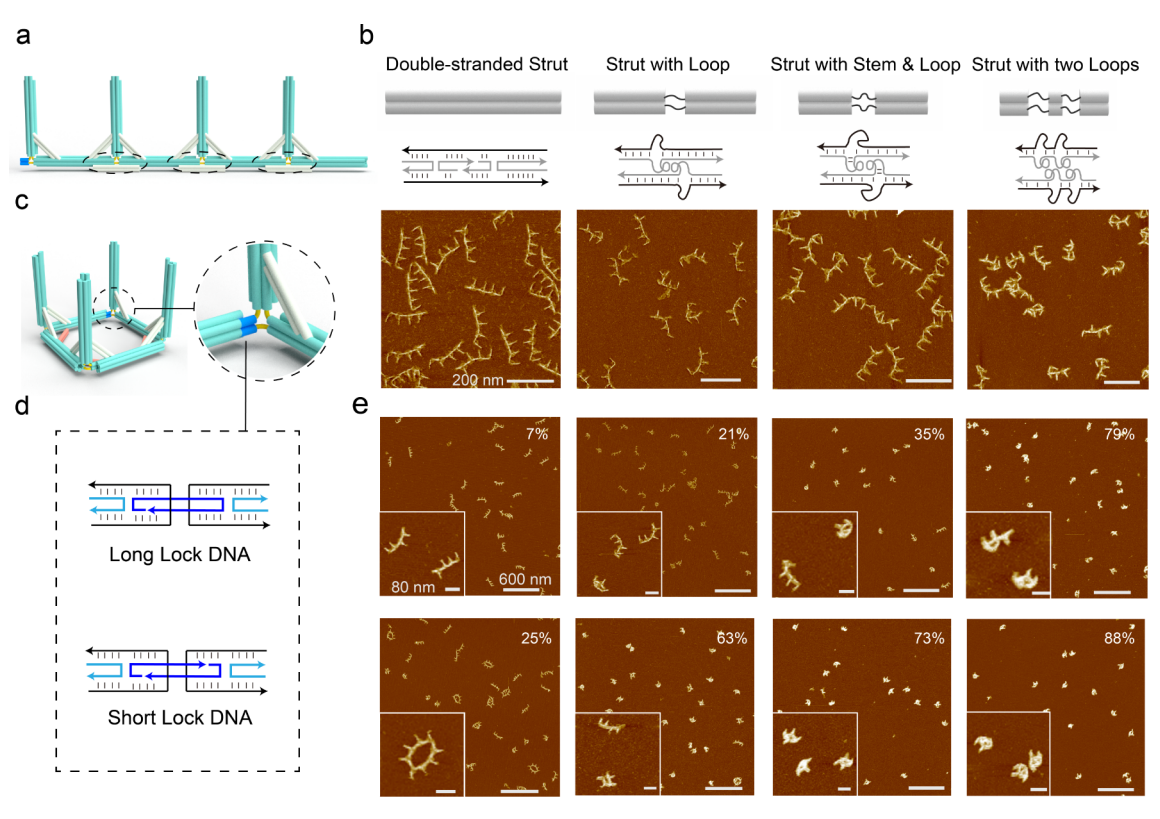


Figure 3. Controlling the configuration of DNA nanocage by the double-stranded level of strut and the length of lock DNA connections. (a) 3D model of the linear branch DNA nanocage. Struts in black dashed circles control linear to square reconfiguration. (b) Four designs of strut with varied hybridization levels, their model representations, pairing sketches and their AFM images. The double-stranded level of strut and straightness level of linear backbone reduce from left to right. Cylinders refer to double-stranded DNA. The length of the loop and stem added on the strut are 21 nucleotides (nt) and 6 base pairings (bp), respectively. Two loops mean two 21-nt loops. The sequence information on staple DNA on the strut can be found Table S3. Scaffold DNA and staple DNA on the strut are labeled in black and silver lines with arrow, respectively. Hydrogen bonds between DNA are represented by two or more short black lines. (c) 3D model of square DNA nanocage and a zoom-in of the conner with lock DNA connection. (d) DNA pairing sketches of Long and Short Lock DNA bridging scaffold, respectively. A long lock staple is broken into two short staples. All Lock DNA are shown in blue and navy lines with arrows and the navy color indicates the one that is broken into two. (e) AFM images of linear branch DNA nanocage with four different strut designs and two look DNA designs. From the left column to the right are of double-stranded design, one loop design, one stem and a loop design, and two loops design, respectively. Long lock DNA connection is added in the four images at the top row, while short lock DNA connection is used at the bottom row. Numbers in images are the yield of square shape out of all folded DNA origami. Scale bar in (b): 200 nm, in (f): 600 nm, in inset images: 80 nm.

arms hanging around appeared more compact than the square shapes under AFM. More AFM images of the one-step reconfigured pyramid DNA nanocage are given in Figure S4. For the transition from the pyramid DNA nanocage to the linear branch shape, we annealed the DNA pyramid nanocage and rearranged its shapes by adding the corresponding open and close sets. Upon addition of the open DNA set, a strutrelaxing conformation was observed (Figure S5). This relaxed DNA nanocage then is hybridized with the close set DNA, fixing all struts to the length and orientation of the linear branch configuration (Figure 2b). The detailed yield calculation of the DNA nanocage and the criteria about differentiating nanocages under AFM were given in Figures S6—S11 and Table S1.

Exploration of Different Strut and Lock DNA Connection Designs. After studying the reconfiguration enabled by struts, we further explored the impact of different types of DNA struts on the shape control of DNA nanocage. DNA struts play a critical role in maintaining the angles between edges, thereby stabilizing the structure of the DNA nanocage. For example, three struts, parallel to the backbone of linear branch DNA nanocage are designed to keep the backbone straight (Figure 3a). If they are relaxed, then the

backbone of our DNA device can easily bend and significantly reduce the homogeneity and the quality control over the assembly, which is one of the key advantages of this approach. To assess this impact, we tested four different designs with varied double-strand level on the backbone struts, including fully double-stranded strut, strut with a 21-nt loop, strut with a 6-bp stem, a 21-nt loop, and strut with two 21-nt loops (Figure 3b). The original design with the highest strut straightness level produced linear branch DNA with the most homogeneous morphology. Regarding the loops on struts, certain sequences designed to be unpaired with the scaffold were added to the strut staples, resulting in loops on both the scaffold and staples. These loops shortened the defined regions on the struts, thereby increasing their flexibility. A 6 bp stem region was designed to assist in and reinforce the formation of the 21-nt loop. Thus, the product of struts with stem and loop was more easily bent than those with a 21-nt loop only. The last design, featuring two 21-nt loops with a total of 42 unpaired nucleotides, exhibited the greatest flexibility in the conformations. The double-stranded level of struts gradually decreased from the first to the last design, leading to morphology changes of the linear branch DNA nanocage observed under AFM (Figure 3b).

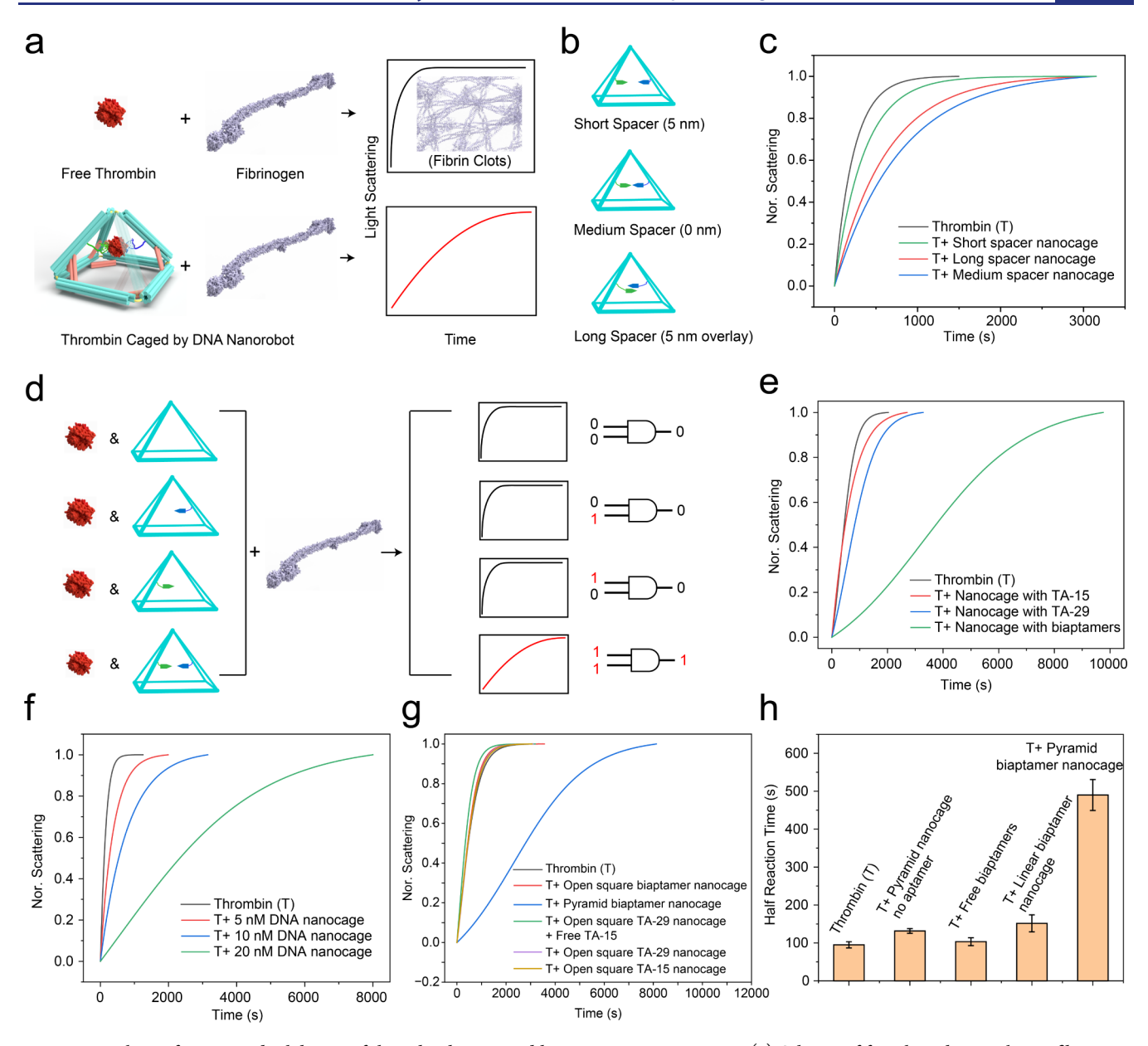


Figure 4. Analysis of caging and inhibition of thrombin by pyramid biaptamer DNA nanocage. (a) Scheme of free thrombin catalyzing fibrinogen to fibrin clots, thrombin inhibition by pyramid DNA nanocages, and corresponding light scattering readouts. To load and inhibit thrombin, biaptamer DNA nanocage is incubated with thrombin prior to mixing with fibrinogen. Thrombin captured by DNA nanocage is inhibited and takes longer time to produce fibrin. The model of fibrinogen is prepared using 3GHG.pdb file. (b) The scheme of DNA nanocage with different distance between two aptamer overhangs. The distance is managed by the number of thymine and calculated by 3.4 nm per 10.5 nt. Short, medium, and long aptamer overhangs, displayed from top to bottom, have 5 nm, 0 nm, and -5 nm (overlay) straight distance between two aptamers, respectively. Blue framework denotes pyramid DNA nanocage and arrowed segments refer to DNA aptamer overhangs. (c) Light scattering measurement of thrombin caged by biaptamer DNA nanocage with short, medium, and long distance between aptamer overhangs. (d) Truth table of pyramid DNA nanocage inhibiting thrombin activity with different aptamers combination. From top to bottom are pyramid DNA nanocage without aptamer, with TA-29 aptamer, with TA-15 aptamer, and with both aptamers. The last combination indicates positive result that inhibits the activity of thrombin. (e) Light scattering measurement of 2.5 nM thrombin incubated with 5 nM nanocage with TA-15 aptamer, with TA-29 aptamer, and with both aptamers. (f) Light scattering measurement of 10 nM thrombin incubated with 5 nM, 10 nM, and 20 nM nanocage. (g) The thrombin activity of control experiments including open square nanocage with biaptamers, with TA-15 only, with TA-29 only and with free TA-15. The concentration of nanocage and free aptamer is 5 nM. The concentration of thrombin is 2.5 nM. (h) The half reaction time of thrombin with different nanocage component. The concentration of thrombin, pyramid nanocage, two free aptamers, linear branch biaptamer nanocage, and pyramid biaptamer nanocage were all 10 nM. Each experiment is carried out three times individually and the error bar is calculated based on the mean value. Curve fitting and normalization are performed for all plotting and information can be found in the Material and Method section in the Supporting Information. Sequences of DNA aptamer staples are listed in Table S4.

The transition between the linear branch and square shape also relies on the design of the lock DNA connections. The lock DNA connection draws the head and tail of the backbone together and stabilizes the square configuration after the strutenabled shape rearrangement (Figure 3c). To study the impact of the lock DNA connections, we compared two designs: one design featuring a single long staple and the other incorporating two shorter staples (Figure 3d). We observed

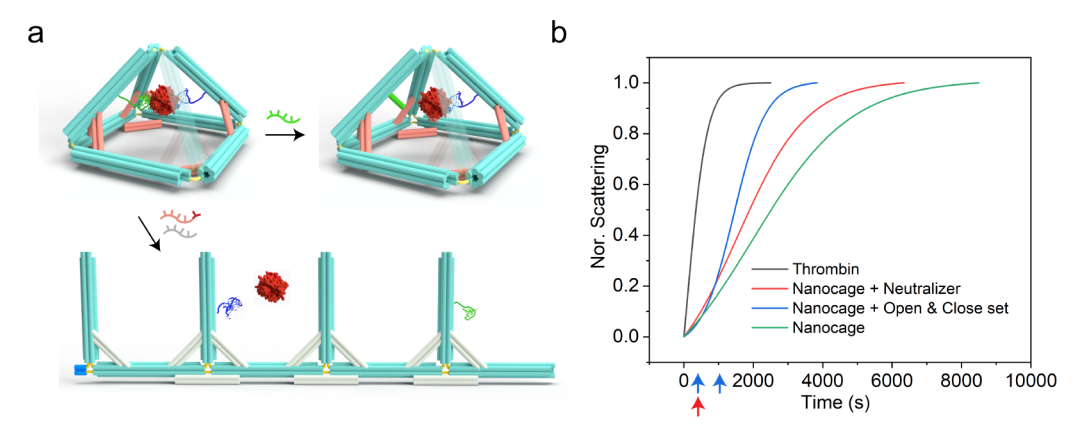


Figure 5. Restoration of thrombin's activity. (a) Schematic representations of thrombin reactivity restoration by adding aptamer neutralizer and by performing reconfiguration. The aptamer neutralizer is a single strand DNA complementary to the TA-15 aptamer (green single strand DNA). It interferes with aptamer-substrate interaction to reverse the inhibition of thrombin. In the second method, reconfiguration, pyramid DNA nanocages respond to the open and close sets DNA and transform to linear branch configuration, releasing thrombin to interact with substrate. (b) Light scattering versus time plotting of thrombin—fibrinogen reaction after adding neutralizer and reconfiguration DNA set to the nanocage captured thrombin. Aptamer neutralizer and open and close sets are added in real-time during the light scattering test. The red arrow to the red curve corresponds to the addition of the aptamer neutralizer strand at 250 s. The blue arrows to the bright curve refer to the adding of the open and close sets at 250 and 1000s, respectively. In both methods, thrombin restores its activity and reaction finishes faster than the positive control, nanocage inhibited thrombin.

that the short lock DNA connections generally yielded more square DNA nanocages than the long lock design in each type of strut design (Figure 3e). The lowest percentage of squared DNA nanocage (\sim 7%) was obtained in the long lock DNA with double-stranded strut group, where most nanostructures remained linear branch shapes. The sample with the same strut design but a shorter lock DNA showed a higher percentage of square shapes (~25%). Notably, eye-shaped dimers (inset image at the bottom left panel of Figure 3e) were observed in this sample. The gel image showed separated bands for the dimer and monomer of the linear branch structure and the squared nanocage (Figure S12). This interesting intermolecular connection emerged from the rigid linear backbone and strong lock connection DNA in this design. With the same lock DNA design, the formation yields of the square nanocages increased when the struts have more unpaired loops. For example, the square nanocages surged to ~79% of the total configurations in the design of long lock DNA with two-loop struts and ~88% in the short lock DNA connections with twoloop struts. A table is made to show the detailed yield information on all samples in Figure 3 (Table S2) and the related AFM images were provided in the Figures S15-S22. This study demonstrates the critical roles of both DNA struts and lock DNA connections in defining the conformations of DNA nanocages and in controlling the reconfiguration process. The gel results of all the combinations of the four different strut designs and the two types of lock DNA connections were provided in Figures S13 and S14.

Encapsulation and Inhibition of Thrombin by DNA Nanocage. Motivated by using DNA nanostructures to regulate proteins, we encapsulated a thrombin protein into the nanocage, leading to the inhibition of thrombin's coagulation activity by bivalent aptamer binding. Our pyramid DNA nanocage offers an inner cavity that can host a sphere of ∼23 nm diameter. Biomolecules and nanoparticles can be anchored inside with the desired locations and orientations after the nanocage is functionalized with targeting moieties. To cage thrombin, we incorporated two well-established DNA aptamers, TA-29 and TA-15, ^{34,35} into the staple DNAs along

the diagonal edges of the DNA pyramid, oriented toward the inside cavity. TA-29 bound to exosite I of thrombin, exhibiting a higher binding affinity, while TA-15 bound to exosite II, acting as a coagulation inhibitor. Our study revealed that the bivalent capture of thrombin inside the pyramid DNA nanocage effectively inhibits thrombin-fibrinogen reaction (Figure 4). Pyramid DNA biaptamer nanocages were first incubated with thrombin to allow encapsulation of thrombin from the environment. The sample was then introduced into a fibrinogen solution for real-time light scattering monitoring by using a fluorometer. Fibrinogen is the natural substrate of thrombin and can be transformed to insoluble fibrin clots. Light scattering measurements can detect these fibrin clots, shown as a sharp, rapidly plateauing curve. In contrast, thrombin captured by DNA biaptamer nanocage is inhibited, resulting in the formation of fibrin clots at a significantly slower rate, shown as a gently ascending curve (Figure 4a).

For effective bivalent aptamer binding, the orientation and distance between the two aptamers are critical. Taking advantage of four DNA six-helix-bundle edges, we can access multiple positions on these four edges facing toward the center of the nanocage. We chose two positions on the diagonal edges to align with the distribution of aptamer binding sites of thrombin, thereby promoting bivalent aptamer binding. In addition to the orientation, the optimal spacing between two aptamers also influences the binding efficiency significantly. To control the distance, a spacer domain is added between the staple sequence and the aptamer sequence. Each aptamer overhang strand consists of three domains: a staple domain that hybridizes with the DNA scaffold, a spacer domain for separation and length control, and an aptamer domain for target binding. Three different spacer designs were tested with distances of 5 nm, 0 nm, and minus 5 nm (indicating a 5 nm overlap) between two aptamers (Figure 4b). Results showed that the nanocage with a medium-length spacer, about 0 nm in distance, exhibited the best thrombin inhibition efficiency (Figure 4c). Following the optimization of the spacer distance, we evaluated the thrombin inhibition by incubating it with different concentrations of DNA nanocage. We observed that

higher nanocage concentrations corresponded to slower fibrin clot formation. Notably, the reaction involving 5 nM thrombin and 20 nM DNA nanocages showed the slowest formation rate among the conditions tested (Figure 4f).

The necessity of having both aptamers on a DNA nanocage to inhibit thrombin generates a logical AND gate. In this system, the DNA biaptamer nanocage inhibits thrombin, and its corresponding light scattering signal is treated as output "1". The absence of any aptamer results in insufficient inhibition against thrombin, showing a "0" output signal (Figure 4d). Our experiments demonstrated that only the DNA nanocage with both aptamers (AND) could effectively inhibit thrombin activity (Figure 4e), indicating that bivalent binding between nanocage and thrombin was the key factor of caging and regulating protein activity. We further tested the half-reaction time of samples containing thrombin and different reagents, including empty (aptamer-free) DNA nanocages, singlestranded free aptamers, and linear branch DNA nanocages modified with aptamers on two branches (Figure 4h). Both samples with empty DNA nanocage and free aptamer strands showed similar results as the thrombin-only sample (a negative control), due to the lack of bivalent binding. For linear branch DNA nanocage, although it contained both aptamers, the unfavored distance/orientation between aptamers and the rigid linear backbone hindered the binding between nanocage and thrombin, leading to a small increase in reaction half time. We also tested control samples, such as open square nanocages with biaptamers, with TA-15 only, and with TA-29 only, and with external free TA-15 added (Figure 4g). All these samples could barely inhibit thrombin, indicating the necessity of thrombin bivalent binding in pyramid nanocage.

Restoring Thrombin's Activity by DNA Nanocage Reconfiguration. Inhibition and activation of protein functions are the two main purposes of protein regulation. After demonstrating the reconfigurable DNA nanocage for encapsulation and inhibition of thrombin, we then explored the strategy to recover its activity, resembling the protein regulation processes by conformational rearrangement in response to molecular triggers. In our system, two approaches were adopted to reactivate the thrombin caged in the reconfigurable DNA device (Figure 5a). One strategy was introducing a DNA strand that was complementary with TA-15 aptamer, named aptamer neutralizer, to compete aptamerprotein binding and release thrombin. The reaction rate of fibrin clotting accelerated after adding the aptamer neutralizer at 250 s, as observed in real-time monitoring (red curve in Figure 5b). The other strategy was to open the DNA nanocage to expose and release the captured protein. By changing the conformation of the DNA nanocage from the pyramid to the linear branch shape, the two aptamers were pulled away from their optimal distances and orientations, therefore releasing the thrombin and restoring its function (Figure 5a). The experimental data showed that the reaction rate increased when reconfiguration strand sets were added at 250 and 1000 s in real-time light scattering and reached the plateau earlier than the other group, indicating the effectiveness of this approach (blue curve in Figure 5b). Raw light scattering data are available in Figure S25.

CONCLUSION

Designing and creating nanodevices for protein regulation offers invaluable tools for biomolecular research and pharmaceutical development. In this study, we presented a reconfigurable DNA nanocage capable of capturing proteins from solutions by multivalent aptamer binding and regulating protein activity by changing configurations in response to molecular triggers. We proved that strutted framework design enabled robust DNA nanostructure assembly and controllable multistage conformation rearrangement. This system is ready to adapt to various proteins. The only module requiring modification is the targeting moieties located within the cavity. For example, antibodies can be modified onto the edges facing the cavity to bind proteins or other targets when aptamers are unavailable. Protein cofactors, agonists, and blockers can be placed within the cavity at the desired number, distance, and orientation to facilitate protein regulation and interaction studies.

This DNA nanocage can be scaled up for larger targets. For example, if one DNA origami folds only a strutted joint of a pyramid, four DNA origami assemble into a larger version of the pyramid nanocage. The higher-order assembly of DNA origami monomers has been demonstrated in previous work, ²⁹ but the dynamic features of the struts are not introduced yet. In this case, the length of the edge will increase from ~40 to ~160 nm, which will be large enough to cage a virus or an exosome, thus enabling antivirus study or exosome analysis.

Finally, computational and signaling modules can be incorporated into the DNA device. As preliminary demonstrated in our work, where an AND logic gate was implemented in the multivalent target recognition and binding processes of this DNA nanocage (Figure 4e,f), other DNA circuits can be introduced, such as a hybridized chain reaction for signal amplification.³⁹ To conclude, the design and functionality of this reconfigurable DNA nanocage for protein encapsulation and regulation contribute to the development of dynamic nanomachines and expand the scope of DNA nanotechnology applications.

ASSOCIATED CONTENT

Supporting Information

The Supporting Information is available free of charge at https://pubs.acs.org/doi/10.1021/jacs.4c06871.

Experiment methods, materials, yield calculations, additional AFM images, gel images, caDNAno diagram of DNA nanocage, criteria for different configurations, and sequence information on DNA aptamers and staples (PDF)

AUTHOR INFORMATION

Corresponding Author

Fei Zhang — Department of Chemistry, Rutgers University, Newark, New Jersey 07102, United States; orcid.org/0000-0002-3177-7547; Phone: 973-353-5520; Email: fei.zhang@rutgers.edu

Authors

Xu Chang – Department of Chemistry, Rutgers University, Newark, New Jersey 07102, United States

Qi Yang — Department of Chemistry, Rutgers University, Newark, New Jersey 07102, United States; ocid.org/ 0000-0001-8005-1112

Jung Yeon Lee – Department of Chemistry, Rutgers University, Newark, New Jersey 07102, United States Devanathan Perumal – Department of Chemistry, Rutgers University, Newark, New Jersey 07102, United States Complete contact information is available at: https://pubs.acs.org/10.1021/jacs.4c06871

Notes

The authors declare no competing financial interest.

ACKNOWLEDGMENTS

This work is supported by a US National Science Foundation (NSF) Faculty Early Career Development Award (DMR-2046835) and a faculty Startup Fund from Rutgers University.

REFERENCES

- (1) Seeman, N. C.; Sleiman, H. F. DNA nanotechnology. *Nat. Rev. Mater.* **2018**, 3 (1), 17068.
- (2) Rothemund, P. W. Folding DNA to create nanoscale shapes and patterns. *Nature* **2006**, 440 (7082), 297–302.
- (3) Douglas, S. M.; Dietz, H.; Liedl, T.; Högberg, B.; Graf, F.; Shih, W. M. Self-assembly of DNA into nanoscale three-dimensional shapes. *Nature* **2009**, 459 (7245), 414–418.
- (4) Huang, C. M.; Kucinic, A.; Johnson, J. A.; Su, H. J.; Castro, C. E. Integrated computer-aided engineering and design for DNA assemblies. *Nat. Mater.* **2021**, *20* (9), 1264–1271.
- (5) Dey, S.; Fan, C.; Gothelf, K. V.; Li, J.; Lin, C.; Liu, L.; Liu, N.; Nijenhuis, M. A. D.; Saccà, B.; Simmel, F. C.; et al. DNA origami. *Nat. Rev. Methods Primers* **2021**, *1* (1), 13.
- (6) Aldaye, F. A.; Palmer, A. L.; Sleiman, H. F. Assembling Materials with DNA as the Guide. *Science* **2008**, 321 (5897), 1795–1799.
- (7) Zhang, F.; Jiang, S.; Wu, S.; Li, Y.; Mao, C.; Liu, Y.; Yan, H. Complex wireframe DNA origami nanostructures with multi-arm junction vertices. *Nat. Nanotechnol.* **2015**, *10* (9), 779–784.
- (8) Hong, F.; Zhang, F.; Liu, Y.; Yan, H. DNA Origami: Scaffolds for Creating Higher Order Structures. *Chem. Rev.* **2017**, *117* (20), 12584–12640.
- (9) Yang, Q.; Chang, X.; Lee, J. Y.; Olivera, T. R.; Saji, M.; Wisniewski, H.; Kim, S.; Zhang, F. Recent Advances in Self-Assembled DNA Nanostructures for Bioimaging. *ACS Appl. Bio Mater.* **2022**, *5*, 4652.
- (10) Chang, X.; Yang, Q.; Lee, J.; Zhang, F. Self-assembled Nucleic Acid Nanostructures for Biomedical Applications. *Curr. Top. Med. Chem.* **2022**, 22 (8), 652–667.
- (11) Yurke, B.; Turberfield, A. J.; Mills, A. P.; Simmel, F. C.; Neumann, J. L. A DNA-fuelled molecular machine made of DNA. *Nature* **2000**, *406* (6796), 605–608.
- (12) Andersen, E. S.; Dong, M.; Nielsen, M. M.; Jahn, K.; Subramani, R.; Mamdouh, W.; Golas, M. M.; Sander, B.; Stark, H.; Oliveira, C. L. P.; et al. Self-assembly of a nanoscale DNA box with a controllable lid. *Nature* **2009**, *459* (7243), 73–76.
- (13) Douglas, S. M.; Bachelet, I.; Church, G. M. A Logic-Gated Nanorobot for Targeted Transport of Molecular Payloads. *Science* **2012**, 335 (6070), 831–834.
- (14) Kuzyk, A.; Schreiber, R.; Zhang, H.; Govorov, A. O.; Liedl, T.; Liu, N. Reconfigurable 3D plasmonic metamolecules. *Nat. Mater.* **2014**, *13* (9), 862–866.
- (15) Bujold, K. E.; Hsu, J. C. C.; Sleiman, H. F. Optimized DNA "Nanosuitcases" for Encapsulation and Conditional Release of siRNA. *J. Am. Chem. Soc.* **2016**, *138* (42), 14030–14038.
- (16) Chang, X.; Zhang, C.; Lv, C.; Sun, Y.; Zhang, M.; Zhao, Y.; Yang, L.; Han, D.; Tan, W. Construction of a Multiple-Aptamer-Based DNA Logic Device on Live Cell Membranes via Associative Toehold Activation for Accurate Cancer Cell Identification. *J. Am. Chem. Soc.* **2019**, *141* (32), 12738–12743.
- (17) Yang, Q.; Chang, X.; Lee, J. Y.; Saji, M.; Zhang, F. DNA T-shaped crossover tiles for 2D tessellation and nanoring reconfiguration. *Nat. Commun.* **2023**, *14* (1), 7675.
- (18) Marras, A. E.; Zhou, L.; Su, H. J.; Castro, C. E. Programmable motion of DNA origami mechanisms. *Proc. Natl. Acad. Sci. U. S. A.* **2015**, *112* (3), 713–718.

- (19) Thubagere, A. J.; Li, W.; Johnson, R. F.; Chen, Z.; Doroudi, S.; Lee, Y. L.; Izatt, G.; Wittman, S.; Srinivas, N.; Woods, D.; Winfree, E.; et al. A cargo-sorting DNA robot. *Science* **2017**, 357 (6356), No. eaan6558.
- (20) Zhang, Y.; Pan, V.; Li, X.; Yang, X.; Li, H.; Wang, P.; Ke, Y. Dynamic DNA Structures. *Small* **2019**, *15* (26), No. e1900228.
- (21) Ramezani, H.; Dietz, H. Building machines with DNA molecules. *Nat. Rev. Genet.* **2020**, 21 (1), 5–26.
- (22) Kuzuya, A.; Sakai, Y.; Yamazaki, T.; Xu, Y.; Komiyama, M. Nanomechanical DNA origami'single-molecule beacons' directly imaged by atomic force microscopy. *Nat. Commun.* **2011**, *2*, 449.
- (23) Kuzyk, A.; Yang, Y.; Duan, X.; Stoll, S.; Govorov, A. O.; Sugiyama, H.; Endo, M.; Liu, N. A light-driven three-dimensional plasmonic nanosystem that translates molecular motion into reversible chiroptical function. *Nat. Commun.* **2016**, *7*, 10591.
- (24) Funck, T.; Nicoli, F.; Kuzyk, A.; Liedl, T. Sensing Picomolar Concentrations of RNA Using Switchable Plasmonic Chirality. *Angew. Chem., Int. Ed.* **2018**, *57* (41), 13495–13498.
- (25) Lund, K.; Manzo, A. J.; Dabby, N.; Michelotti, N.; Johnson-Buck, A.; Nangreave, J.; Taylor, S.; Pei, R.; Stojanovic, M. N.; Walter, N. G.; et al. Molecular robots guided by prescriptive landscapes. *Nature* **2010**, *465* (7295), 206–210.
- (26) Grossi, G.; Dalgaard Ebbesen Jepsen, M.; Kjems, J.; Andersen, E. S. Control of enzyme reactions by a reconfigurable DNA nanovault. *Nat. Commun.* **2017**, 8 (1), 992.
- (27) Li, S.; Jiang, Q.; Liu, S.; Zhang, Y.; Tian, Y.; Song, C.; Wang, J.; Zou, Y.; Anderson, G. J.; Han, J. Y.; et al. A DNA nanorobot functions as a cancer therapeutic in response to a molecular trigger in vivo. *Nat. Biotechnol.* **2018**, *36* (3), 258–264.
- (28) Sigl, C.; Willner, E. M.; Engelen, W.; Kretzmann, J. A.; Sachenbacher, K.; Liedl, A.; Kolbe, F.; Wilsch, F.; Aghvami, S. A.; Protzer, U.; et al. Programmable icosahedral shell system for virus trapping. *Nat. Mater.* **2021**, 20 (9), 1281–1289.
- (29) Iinuma, R.; Ke, Y.; Jungmann, R.; Schlichthaerle, T.; Woehrstein, J. B.; Yin, P. Polyhedra Self-Assembled from DNA Tripods and Characterized with 3D DNA-PAINT. *Science* **2014**, 344 (6179), 65–69.
- (30) Ke, Y.; Meyer, T.; Shih, W. M.; Bellot, G. Regulation at a distance of biomolecular interactions using a DNA origami nanoactuator. *Nat. Commun.* **2016**, *7*, 10935.
- (31) Kim, Y.; Cao, Z.; Tan, W. Molecular assembly for high-performance bivalent nucleic acid inhibitor. *Proc. Natl. Acad. Sci. U. S. A.* **2008**, *105* (15), 5664–5669.
- (32) Yang, L.; Zhao, Y.; Xu, X.; Xu, K.; Zhang, M.; Huang, K.; Kang, H.; Lin, H. C.; Yang, Y.; Han, D. An Intelligent DNA Nanorobot for Autonomous Anticoagulation. *Angew. Chem., Int. Ed.* **2020**, 59 (40), 17697–17704.
- (33) Hu, X.; Tang, L.; Zheng, M.; Liu, J.; Zhang, Z.; Li, Z.; Yang, Q.; Xiang, S.; Fang, L.; Ren, Q.; et al. Structure-Guided Designing Pre-Organization in Bivalent Aptamers. *J. Am. Chem. Soc.* **2022**, *144* (10), 4507–4514.
- (34) Bock, L. C.; Griffin, L. C.; Latham, J. A.; Vermaas, E. H.; Toole, J. J. Selection of single-stranded DNA molecules that bind and inhibit human thrombin. *Nature* **1992**, *355* (6360), 564–566.
- (35) Tasset, D. M.; Kubik, M. F.; Steiner, W. Oligonucleotide inhibitors of human thrombin that bind distinct epitopes. *J. Mol. Biol.* **1997**, 272 (5), 688–698.
- (36) Berezovski, M.; Nutiu, R.; Li, Y.; Krylov, S. N. Affinity Analysis of a Protein–Aptamer Complex Using Nonequilibrium Capillary Electrophoresis of Equilibrium Mixtures. *Anal. Chem.* **2003**, *75* (6), 1382–1386.
- (37) Rinker, S.; Ke, Y.; Liu, Y.; Chhabra, R.; Yan, H. Self-assembled DNA nanostructures for distance-dependent multivalent ligand-protein binding. *Nat. Nanotechnol.* **2008**, *3* (7), 418–422.
- (38) Tikhomirov, G.; Petersen, P.; Qian, L. Triangular DNA Origami Tilings. *J. Am. Chem. Soc.* **2018**, *140* (50), 17361–17364.
- (39) Dirks, R. M.; Pierce, N. A. Triggered amplification by hybridization chain reaction. *Proc. Natl. Acad. Sci. U. S. A.* **2004**, *101* (43), 15275–15278.